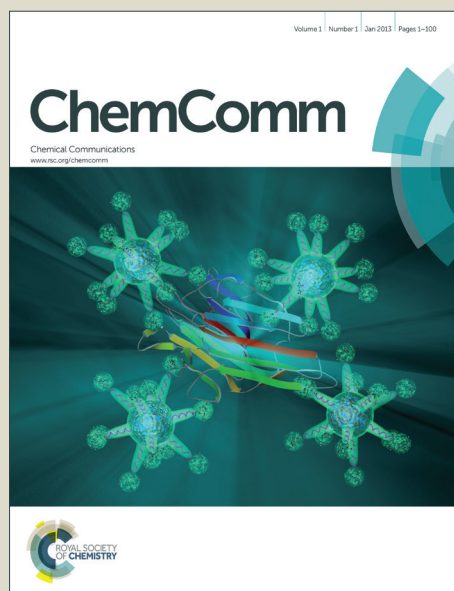


# ChemComm

Accepted Manuscript



This is an *Accepted Manuscript*, which has been through the Royal Society of Chemistry peer review process and has been accepted for publication.

*Accepted Manuscripts* are published online shortly after acceptance, before technical editing, formatting and proof reading. Using this free service, authors can make their results available to the community, in citable form, before we publish the edited article. We will replace this *Accepted Manuscript* with the edited and formatted *Advance Article* as soon as it is available.

You can find more information about *Accepted Manuscripts* in the [Information for Authors](#).

Please note that technical editing may introduce minor changes to the text and/or graphics, which may alter content. The journal's standard [Terms & Conditions](#) and the [Ethical guidelines](#) still apply. In no event shall the Royal Society of Chemistry be held responsible for any errors or omissions in this *Accepted Manuscript* or any consequences arising from the use of any information it contains.

Cite this: DOI: 10.1039/c0xx00000x

www.rsc.org/xxxxxx

**ARTICLE TYPE**

## Self-Assembled Organic Monolayers on Epitaxial Graphene with Enhanced Structural and Thermal Stability

Hunter J. Karmel,<sup>a</sup> John J. Garramone,<sup>a</sup> Jonathan D. Emery,<sup>a</sup> Sumit Kewalramani,<sup>a</sup> Michael J. Bedzyk,<sup>a,b</sup> and Mark C. Hersam<sup>\*,a,c</sup>

5 Received (in XXX, XXX) Xth XXXXXXXXX 20XX, Accepted Xth XXXXXXXXX 20XX  
DOI: 10.1039/b000000x

Scanning tunnelling microscopy and X-ray reflectivity are used to characterize adlayers of perylenetetracarboxylic diimide (PTCDI) deposited on epitaxial graphene (EG) on SiC(0001). PTCDI adopts a herringbone structural phase on EG/SiC that can accommodate sub-5 nm voids with molecularly defined boundaries and isolated molecular vacancies at room temperature. The PTCDI monolayer remains intact up to substrate temperatures of ~260 °C, thus demonstrating enhanced thermal stability compared to previously studied perylene derivatives on EG/SiC.

Carbon-based nanomaterials and organic semiconductors have emerged independently as promising candidates for next-generation electronic materials due to their outstanding carrier mobilities and highly-tunable energy band structures, respectively. In particular, graphene, an atomically thin hexagonal lattice of *sp*<sup>2</sup>-hybridized carbon atoms, has attracted significant interest from a diverse array of scientific disciplines as a result of its combination of exceptional physical and chemical properties.<sup>1-2</sup> Similarly, perylene derivatives have been the subject of intense study as a result of their versatile self-assembly characteristics,<sup>3-8</sup> suitability for a wide range of processing schemes,<sup>4-5, 9-12</sup> and the relative ease with which they can be modified chemically for specific applications.<sup>13-14</sup> Given the complementary nature of these inherently distinct sets of attributes, the integration of these two materials has been the subject of recent theoretical<sup>15-16</sup> and experimental investigations.<sup>7-8, 17-22</sup> However, many issues relating to the structural and thermal stability of these graphene-organic interfaces have yet to be fully addressed. Consequently, the identification of non-covalently interacting molecular adsorbates, which form energetically stable configurations on graphene at and above room temperature, remains an issue of both fundamental and practical importance.

Despite its superlative properties, pristine graphene suffers from several inherent limitations that hinder its overall utility. Foremost among these is its lack of a band gap, which has frustrated progress in the development of graphene-based digital electronics. Additionally, the chemically inert nature of the graphitic basal plane has inhibited the integration of graphene with other technologically-relevant materials.<sup>23</sup> In order to overcome these obstacles, the graphene research community has sought reliable approaches to modulate the intrinsic electronic

and chemical behavior of graphene through the use of covalent<sup>24-28</sup> and non-covalent adsorbates.<sup>7-8, 15-21, 29-32</sup> To characterize these surface functionalization schemes, ultra-high vacuum (UHV) scanning tunneling microscopy (STM) has been particularly useful due to its sensitivity to both the electronic and topographic features of surfaces at the atomic-scale.<sup>7-8, 17-18, 21, 25, 30</sup>

One especially intriguing category of small organic molecules that is known to possess excellent thermal and photochemical stability is the class of perylene derivatives.<sup>13</sup> Among these compounds, perylenetetracarboxylic diimide (PTCDI) serves as the elementary building block from which the vast majority of these derivatives have been synthesized.<sup>13-14</sup> Recent reports have further suggested that  $\pi$ - $\pi$  stacking interactions with polycyclic aromatic molecules, such as PTCDI, may be useful for doping and band gap engineering of graphene substrates.<sup>15-16, 19</sup>

In this communication, we present a UHV STM investigation of the formation and molecular self-organization characteristics of PTCDI monolayers on epitaxial graphene (EG) on SiC(0001) at room temperature. The molecule-substrate and intermolecular interactions governing this system are found to promote structural stability as evidenced by highly-ordered boundaries between PTCDI molecular islands and neighboring regions of exposed graphene. To quantify the thermal stability of the PTCDI monolayer, temperature-dependent X-ray reflectivity (XRR) analysis is performed to compare the relative adsorption strength of both PTCDI and the previously studied perylene derivative on EG/SiC: 3,4,9,10-perylenetetracarboxylic dianhydride (PTCDA). Specifically, we find that the onset of thermal desorption takes place at a temperature  $38 \pm 10$  °C higher for PTCDI compared to PTCDA. Overall, this study demonstrates that PTCDI is an exceptionally stable organic monolayer on EG, suggesting its use for chemical functionalization in graphene-based technologies.

STM characterization and sample preparation were performed using a home-built room temperature UHV STM system with a base pressure of  $\sim 6 \times 10^{-11}$  Torr.<sup>33</sup> Topographic STM imaging was conducted in constant-current mode where the samples were biased with respect to electrochemically etched tungsten probes. Following graphitization of SiC(0001) via thermal annealing at  $\sim 1325$  °C for 10 min, the resulting atomically pristine surfaces were observed to consist of a mixture of monolayer and bilayer EG regions, as shown in Figs. 1a and 1b. The EG substrate was maintained at room temperature during the molecular deposition of PTCDI, illustrated schematically in Fig. 1c, and subsequently

annealed at 60 °C for 1 hour to promote the formation of uniform and well-ordered molecular adlayers, depicted schematically in Fig. 1d (additional sample preparation details are provided in the Supplementary Information (SI)). The characteristics of these homomolecular PTCDI adlayers were then explored at the molecular-scale via STM, as shown in Figs. 1e and 1f, where the detailed structural relationships between individual molecules of the 2D supramolecular architecture could be readily identified.

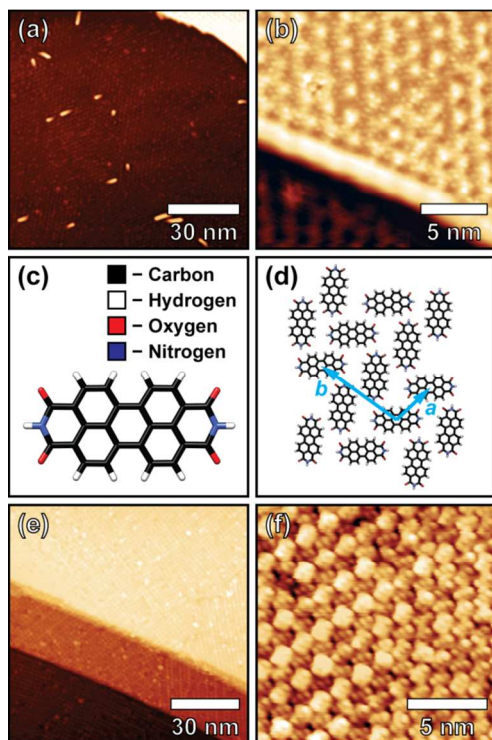


**Fig. 1** (a) STM image of EG/SiC(0001) (sample bias ( $V_s$ ) = -2.0 V; tunneling current ( $I_t$ ) = 0.08 nA). (b) STM image of monolayer graphene where the underlying ( $6\sqrt{3} \times 6\sqrt{3}$ )R30° structure is visible as an array of bright protrusions ( $V_s$  = -1.0 V;  $I_t$  = 0.08 nA). (c) Structure of PTCDI. (d) Schematic of the PTCDI herringbone motif, with lattice vectors **a** and **b**. (e) STM image acquired following the deposition of a PTCDI monolayer ( $V_s$  = -1.0 V;  $I_t$  = 0.05 nA). (f) Molecular-resolution STM image of the PTCDI monolayer ( $V_s$  = -1.0 V;  $I_t$  = 0.04 nA).

As shown in Fig. 1e, PTCDI forms a densely-packed 2D self-assembled molecular adlayer with characteristic domain sizes exceeding 100 nm. These molecular domains extend smoothly over the underlying EG/SiC(0001) substrate and traverse potentially disruptive topographic features including step edges and surface defects. STM images with sub-molecular resolution, such as Fig. 1f, reveal the detailed structural arrangement of each PTCDI molecule within the adlayer. In particular, a new herringbone phase for PTCDI is observed that has not been previously demonstrated experimentally. This herringbone assembly has been theoretically predicted as one of six architecturally distinct monolayers based upon PTCDI dimers.<sup>6</sup> A qualitative schematic diagram of the PTCDI herringbone phase is depicted in Fig. 1d, where the lattice vectors **a** and **b** are identified. The measured lengths of these lattice vectors and the angle between them, as assessed in Fig. 1f, are found to be: **a** =  $1.53 \pm 0.02$  nm, **b** =  $1.89 \pm 0.01$  nm, and  $\gamma$  =  $97.5 \pm 2.5^\circ$ . In a manner analogous to what has been previously documented for

PTCDA on EG/SiC(0001),<sup>17</sup> PTCDI molecules at the corner sites of the unit cell display a different topographic contrast in STM images than the molecules at the center of the cell. This disparate contrast results in the development of corresponding brighter and darker stripes of molecules that are aligned along the **a** vector.

This molecular arrangement of PTCDI on EG/SiC(0001) differs significantly from the structures that have been observed on graphite substrates<sup>4</sup> or heteroepitaxial graphene thin films grown on Rh(111).<sup>21</sup> On HOPG, PTCDI has been shown to self-assemble into adjacent parallel rows with the individual molecules within each row arranged at a slightly canted angle with respect to their neighbors.<sup>4</sup> On the other hand, recent work has demonstrated that PTCDI forms structurally stable, spatially separated, one-dimensional rows on EG/Rh(111), where each chain is one molecule wide.<sup>21</sup> Evidently, the ordering of PTCDI on graphene depends strongly on the corrugation, topography, and electronic properties of the underlying substrate.

Examination of the structure of PTCDI assemblies at sub-monolayer coverage indicates that the 2D molecular domains exhibit a high degree of structural stability under routine scanning conditions. As shown in Fig. SI-2a, the PTCDI island transitions abruptly into a clean graphene region on an otherwise atomically flat terrace. At higher resolution (Fig. SI-2c), it is apparent that these molecularly-defined edges can occur on any side of the 2D molecular crystal, thereby permitting the formation of arbitrarily shaped boundaries.

The stability of PTCDI domain edges is in stark contrast with similar self-assembled molecular structures formed on identically prepared substrates. For example, previous work with PTCDA showed the formation of 2D molecular islands with disordered domain boundaries.<sup>17-18</sup> The edge instability observed for PTCDA was attributed to a combination of thermal factors and STM tip interactions during scanning. However, PTCDI molecules are known to have stronger homomolecular hydrogen bonding interactions than PTCDA.<sup>6</sup> The observed stabilization of the well-ordered PTCDI island edge structure at room temperature may therefore be the result of the comparatively strong NH...O intermolecular hydrogen bonds that form between neighboring PTCDI molecules. An associated consequence of this stable edge behavior is that molecularly-defined void structures exhibit similar stability, as shown in Fig. 2. A range of void structures have been observed including diamond-shaped voids (Fig. 2a), rectangular voids (Fig. 2b), and individual molecular vacancies (Fig. 2c). In addition we note that Fig. 2c exhibits a different molecular ordering than the typically observed herringbone architecture on EG/SiC(0001). Instead, this region of the surface has self-organized into a canted molecular phase similar to that observed on HOPG.

Following room temperature STM characterization of the PTCDI molecular adlayer structural stability, the relative thermal stability of PTCDI and PTCDA adlayers on EG/SiC(0001) was quantified using XRR, a measurement sensitive to the coverage of the molecular overlayer (XRR experimental details and supplementary data are provided in the SI).<sup>22</sup> Fig. SI-3 shows temperature-dependent high-resolution XRR for EG/SiC(0001), PTCDA/EG/SiC(0001), and PTCDI/EG/SiC(0001) samples at

$$L = 2 \sin\left(\frac{2\theta}{2}\right) \frac{c_{SiC}}{\lambda} \approx 4.5 \text{ SiC reciprocal lattice units (SiC r.l.u.)},$$

which corresponds to the  $d$ -spacing of graphite (0002) ( $d \approx 3.35 \text{ \AA}$ ). Here,  $2\theta$  is the scattering angle,  $\lambda = 0.827 \text{ \AA}$  is the X-ray wavelength, and  $c_{\text{SiC}} = 15.12 \text{ \AA}$  is the lattice parameter for 6H-SiC. Each dataset exhibits a strong, sharp SiC(0006) single-crystal diffraction peak at  $L = 6.0 \text{ SiC r.l.u.}$ , as well as a broader, weaker signal at  $L \approx 4.5 \text{ SiC r.l.u.}$  from the combined contributions of the EG and  $\pi$ -stacked molecular layers.<sup>22</sup> As both samples are heated, the film peak irreversibly reduces in integrated intensity, broadens, and shifts to lower  $L$  (Fig. SI-3). This behavior is indicative of an adlayer that is decreasing in layer occupancy and total thickness, as well as increasing in average  $d$ -spacing, thereby reverting to a bare EG/SiC(0001) film. The heating in vacuum of bare EG/SiC(0001), in contrast, has little effect on the scattered intensity (Fig. 3), and thus the behavior for PTCDI and PTCDA is indicative of the desorption of the organic monolayer. A weak temperature-dependent decrease in intensity is observable for all samples prior to the main thermal desorption events and is attributed to an increase in the Debye-Waller factor with temperature.

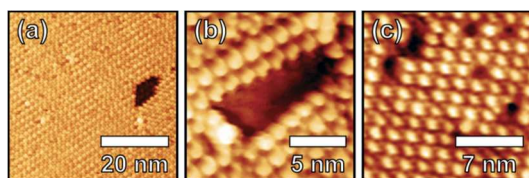


**Fig. 2** (a) STM image of a diamond-shaped molecular void located within a PTCDI monolayer ( $V_s = -1.0 \text{ V}$ ;  $I_t = 0.04 \text{ nA}$ ). (b) STM image of a rectangular molecular void located on the interior of an individual PTCDI domain ( $V_s = -1.1 \text{ V}$ ;  $I_t = 0.03 \text{ nA}$ ). (c) STM image of a PTCDI island with an array of isolated molecular vacancies ( $V_s = -1.3 \text{ V}$ ;  $I_t = 0.03 \text{ nA}$ ).

Full quantitative analysis of the XRR data at each temperature can be used to evaluate the PTCDA and PTCDI coverage as a function of temperature.<sup>22</sup> However, a simpler and more direct approach for assessing the molecular coverage,  $\Theta(T)$ , at temperature  $T$ , is to monitor the square root of the intensity,  $\sqrt{I(L, T)}$ , at the  $L$  value associated with the  $d$ -spacing of the overlying molecular thin film ( $L \approx 4.5 \text{ SiC r.l.u.}$ , corresponding to  $d \approx 3.35 \text{ \AA}$ ). Details on this method, which is based on Redhead thermal desorption analysis, are provided in the SI.<sup>34</sup> A plot of  $\sqrt{I(4.5, T)}$  [correlated with  $\Theta(T)$ ] is shown in Fig. 3, and arrows indicate the transition temperature  $T_c$  at the inflection point of the fitted Gauss error function. With this definition, we find that the  $T_c$  for PTCDA and PTCDI is  $223 \pm 5 \text{ }^\circ\text{C}$  and  $261 \pm 5 \text{ }^\circ\text{C}$ , respectively. The final  $\sqrt{I(L, T)}$  values, which are essentially identical to bare EG/SiC(0001), differ slightly due to small variations in graphene coverage between samples.

In summary, the structural and thermal properties of a densely-packed hydrogen-bonded PTCDI adlayer have been investigated on EG/SiC(0001). The structural stability of the PTCDI adlayer allows for molecularly defined domain boundaries, voids, and vacancies at room temperature. The thermal desorption properties of the PTCDI monolayer is assessed in comparison to the closely related PTCDA molecule, where we find that PTCDI desorbs at a temperature  $38 \pm 10 \text{ }^\circ\text{C}$  higher than PTCDA. Overall, these results provide insight into the subtle chemical and interfacial factors that influence the stability of molecular adlayers on EG and thus provide guidance for the controlled fabrication of organo-graphene nanostructures.

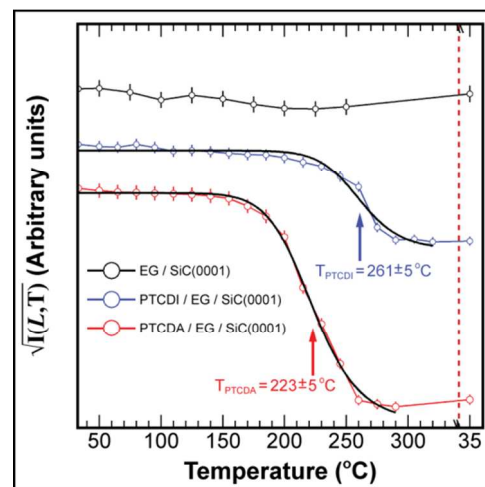


**Fig. 3** From XRR experiments,  $\sqrt{I(L, T)}$  at  $L = 4.5 \text{ r.l.u.}$  provides a measurement of the PTCDA and PTCDI coverage as a function of increasing substrate temperature. The desorption temperature, which is an indication of the PTCDA and PTCDI adsorption energies, is defined as the inflection point of the  $\sqrt{I(4.5, T)}$  curve for each organic adlayer. A post-desorption room temperature control measurement is provided to the right of the dashed line. Plots are offset for clarity.

This work was supported by the NSF-MRSEC (DMR-1121262), DOE (DE-FG02-09ER16109), ONR (N00014-11-1-0463), AFOSR (FA9550-11-1-0275), and Keck Foundation. XRR was performed at the Advanced Photon Source at Argonne National Laboratory, which is funded by DOE (DE-AC02-06CH11357) using the DND-CAT 5ID-C station supported by DuPont, Northwestern University, and Dow Chemical.

## Notes and references

- \*E-mail: m-hersam@northwestern.edu  
<sup>a</sup> Dept. of Materials Science & Engineering, Northwestern Univ., Evanston, IL 60208, USA  
<sup>b</sup> Dept. of Physics, Northwestern Univ., Evanston, IL 60208, USA  
<sup>c</sup> Dept. of Chemistry, Northwestern Univ., Evanston, IL 60208, USA  
<sup>†</sup> Electronic Supplementary Information (ESI) available: [sample preparation; STM, XRR characterization]. See DOI: 10.1039/b000000x/
1. A. K. Geim and K. S. Novoselov, *Nat Mater*, 2007, **6**, 183-191.
  2. A. K. Geim, *Science*, 2009, **324**, 1530-1534.
  3. F. Silly, A. Q. Shaw, M. R. Castell and G. A. D. Briggs, *Chem Commun*, 2008, 1907-1909.
  4. C. Ludwig, B. Gompf, J. Petersen, R. Strohmaier and W. Eisenmenger, *Z Phys B Con Mat*, 1994, **93**, 365-373.
  5. R. Madueno, M. T. Raisanen, C. Silien and M. Buck, *Nature*, 2008, **454**, 618-621.
  6. M. Mura, F. Silly, G. A. D. Briggs, M. R. Castell and L. N. Kantorovich, *J Phys Chem C*, 2009, **113**, 21840-21848.
  7. H. Yang, A. J. Mayne, G. Comtet, G. Dujardin, Y. Kuk, P. Sonnet, L. Stauffer, S. Nagarajan and A. Gourdon, *Phys Chem Chem Phys*, 2013, **15**, 4939-4946.
  8. H. J. Karmel, T. Y. Chien, V. Demers-Carpentier, J. J. Garramone and M. C. Hersam, *J Phys Chem Lett*, 2014, **5**, 270-274.
  9. W. Su, Y. X. Zhang, C. T. Zhao, X. Y. Li and J. Z. Jiang, *Chemphyschem*, 2007, **8**, 1857-1862.
  10. T. V. Desai, E. R. Kish, A. R. Woll and J. R. Engstrom, *J Phys Chem C*, 2011, **115**, 18221-18234.

11. Q. Chen, B. J. Worfolk, T. C. Hauger, U. Al-Atar, K. D. Harris and J. M. Buriak, *ACS Appl Mater Inter*, 2011, **3**, 3962-3970.
12. T. Rothlaender, U. Palfinger, B. Stadlober, A. Haase, H. Gold, C. Palfinger, G. Domann, J. Kraxner, G. Jakopic and P. Hartmann, *J Mater Res*, 2011, **26**, 2470-2478.
13. H. Icil and E. Arslan, *Spectrosc Lett*, 2001, **34**, 355-363.
14. M. C. R. Delgado, E. G. Kim, D. A. da Silva and J. L. Bredas, *J Am Chem Soc*, 2010, **132**, 3375-3387.
15. S. M. Kozlov, F. Vines and A. Gorling, *Adv Mater*, 2011, **23**, 2638-2643.
16. S. M. Kozlov, F. Vines and A. Gorling, *Carbon*, 2012, **50**, 2482-2492.
17. Q. H. Wang and M. C. Hersam, *Nat Chem*, 2009, **1**, 206-211.
18. Q. H. Wang and M. C. Hersam, *Nano Lett*, 2011, **11**, 589-593.
19. Z. X. Zhang, H. L. Huang, X. M. Yang and L. Zang, *J Phys Chem Lett*, 2011, **2**, 2897-2905.
20. J. E. Johns, H. J. Karmel, J. M. P. Alaboson and M. C. Hersam, *J Phys Chem Lett*, 2012, **3**, 1974-1979.
21. A. J. Pollard, E. W. Perkins, N. A. Smith, A. Saywell, G. Goretzki, A. G. Phillips, S. P. Argent, H. Sachdev, F. Muller, S. Hufner, S. Gsell, M. Fischer, M. Schreck, J. Osterwalder, T. Greber, S. Berner, N. R. Champness and P. H. Beton, *Angew Chem Int Edit*, 2010, **49**, 1794-1799.
22. J. D. Emery, Q. H. Wang, M. Zarrouati, P. Fenter, M. C. Hersam and M. J. Bedzyk, *Surf Sci*, 2011, **605**, 1685-1693.
23. J. A. Robinson, M. LaBella, K. A. Trumbull, X. J. Weng, R. Cavelero, T. Daniels, Z. Hughes, M. Hollander, M. Fanton and D. Snyder, *ACS Nano*, 2010, **4**, 2667-2672.
24. M. Z. Hossain, M. A. Walsh and M. C. Hersam, *J Am Chem Soc*, 2010, **132**, 15399-15403.
25. M. Z. Hossain, J. E. Johns, K. H. Bevan, H. J. Karmel, Y. T. Liang, S. Yoshimoto, K. Mukai, T. Koitaya, J. Yoshinobu, M. Kawai, A. M. Lear, L. L. Kesmodel, S. L. Tait and M. C. Hersam, *Nat Chem*, 2012, **4**, 305-309.
26. J. E. Johns and M. C. Hersam, *Accounts Chem Res*, 2013, **46**, 77-86.
27. J. E. Johns, J. M. P. Alaboson, S. Patwardhan, C. R. Ryder, G. C. Schatz and M. C. Hersam, *J Am Chem Soc*, 2013, **135**, 18121-18125.
28. E. C. Mattson, J. E. Johns, K. Pande, R. A. Bosch, S. Cui, M. Gajdardziska-Josifovska, M. Weinert, J. H. Chen, M. C. Hersam and C. J. Hirschmugl, *J Phys Chem Lett*, 2014, **5**, 212-219.
29. J. M. P. Alaboson, Q. H. Wang, J. D. Emery, A. L. Lipson, M. J. Bedzyk, J. W. Elam, M. J. Pellin and M. C. Hersam, *ACS Nano*, 2011, **5**, 5223-5232.
30. A. Deshpande, C. H. Sham, J. M. P. Alaboson, J. M. Mullin, G. C. Schatz and M. C. Hersam, *J Am Chem Soc*, 2012, **134**, 16759-16764.
31. V. K. Sangwan, D. Jariwala, S. A. Filippone, H. J. Karmel, J. E. Johns, J. M. P. Alaboson, T. J. Marks, L. J. Lauhon and M. C. Hersam, *Nano Lett*, 2013, **13**, 1162-1167.
32. J. M. P. Alaboson, C. H. Sham, S. Kewalramani, J. D. Emery, J. E. Johns, A. Deshpande, T. Y. Chien, M. J. Bedzyk, J. W. Elam, M. J. Pellin and M. C. Hersam, *Nano Lett*, 2013, **13**, 5763-5770.
33. E. T. Foley, N. L. Yoder, N. P. Guisinger and M. C. Hersam, *Rev Sci Instrum*, 2004, **75**, 5280-5287.
34. P. A. Redhead, *Vacuum*, 1962, 203-211.